

## COMBINED METHOD FOR THE COMPUTATION OF THE DOUBLY PERIODIC GREEN'S FUNCTION

N. Guérin, S. Enoch, and G. Tayeb

Institut Fresnel  
Faculté des Sciences et Techniques de Saint-Jérôme  
Case 262, 13397 Marseille Cedex 20, France

**Abstract**—The performances of several methods used for the computation of the free space Green's function for doubly periodic arrays are investigated. We make a careful study of these methods, based on accuracy and computing time criteria. We show that none of them is able to fulfil both criteria for a large range of parameters (position in space, wavelength, periods, ...). Fortunately, it is possible to retain three complementary algorithms. We combine them in order to implement a numerical code that automatically chooses the appropriate algorithm depending on the parameters.

### 1 Introduction

### 2 Expression of the Green's Function

#### 2.1 Spatial Form

#### 2.2 Spectral Form

#### 2.3 First Mixed Form Starting from Spatial Form

#### 2.4 Second Mixed Form Starting from Spectral Form

### 3 Numerical Study

#### 3.1 Shanks' Transform

#### 3.2 Optimization of the Parameters $u$ and $v$

#### 3.3 Numerical Comparison of the Methods

### 4 Conclusion

### Appendix

### References

## 1. INTRODUCTION

Three-dimensional electromagnetic problems require huge computing resources. One way to go through is to consider periodic structures in order to reduce the investigation domain to one cell of the structure. Many numerical methods, such as integral methods, require the computation of a Green's function. Unfortunately, the more straightforward expressions of periodic Green's functions lead to very slow converging series. Numerous works have been devoted to the Green's function for one-dimensional gratings. The acceleration of the convergence can result from different transformations: Kummer's transform [1–3] combined with Poisson's transform [4], numerical non linear transforms such as Shanks [5], Levin [6] or  $\rho$ -transform [7]. An alternative solution is to use the so-called Lattice Sums [1, 8]. Here, we focus on the efficient computation of the Green's function for doubly periodic arrays (used for instance in crossed grating problems). Fewer works concern this problem. At the present time, and in collaboration with the Sydrey group (R. McPhedran, N. Nicorovici, L. Botten, J. Nixon), we investigate developments of the Lattice Sums method. This method has a heavy computational burden to calculate the lattice sums, but the calculation of the Green's function is there after quite quick for each field point. In this paper, we combine the techniques reported in the earlier studies by Jorgenson et al. [4] and by Singh et al. [9]. By this way, we obtain different methods to compute this Green's function. None of these methods is optimum for all positions of the observation point. A systematic numerical study allows us to define the regions of space where each method offers the best performances. Compared to the Lattice Sums method, the combined method presented in this paper has a computational burden which increases linearly with the number of field points. The resulting Fortran subroutine (freely downloadable [10]) takes these considerations into account in order to choose automatically the most efficient method.

## 2. EXPRESSION OF THE GREEN'S FUNCTION

### 2.1. Spatial Form

The doubly periodic Green's function  $G(x, y, z)$  under investigation is the solution verifying an outgoing wave condition of the inhomogeneous Helmholtz equation:

$$(\Delta + k^2)G(x, y, z)$$

$$= \delta(z) \sum_{n=-\infty}^{+\infty} \sum_{m=-\infty}^{+\infty} \delta(x - nd_x) \delta(y - md_y) \exp(i\alpha_0 nd_x + i\beta_0 md_y) \quad (1)$$

where  $k$  is the wave number ( $k^2 \in \mathbb{R}$ ),  $d_x$  and  $d_y$  are the periods on the  $x$  and  $y$  axes,  $\alpha_0$  and  $\beta_0$  are the pseudo-periodicity coefficients. In all the paper, we use an orthogonal coordinate system  $(O, x, y, z)$ . Note that in the underlying electromagnetic problem, the harmonic fields are represented using a time dependence in  $\exp(-i\omega t)$ . This remark is important for the expression of the outgoing wave condition. The spatial form of  $G(x, y, z)$  is obtained directly from the elementary solution of  $(\Delta + k^2)g(x, y, z) = \delta(x, y, z)$ , i.e., the free-space Green's function  $-\exp(ikr)/(4\pi r)$ , and writes:

$$G(x, y, z) = -\frac{1}{4\pi} \sum_{n=-\infty}^{+\infty} \sum_{m=-\infty}^{+\infty} \frac{\exp(ikr_{nm})}{r_{nm}} \exp(i\alpha_0 nd_x + i\beta_0 md_y) \quad (2)$$

where  $r_{nm}$  is the distance from the "source" located at point  $(nd_x, md_y, 0)$  to the observation point  $(x, y, z)$ :

$$r_{nm} = \sqrt{(x - nd_x)^2 + (y - md_y)^2 + z^2} \quad (3)$$

## 2.2. Spectral Form

From classical calculus using Fourier series, we get from (1) another expansion for  $G$  (see Appendix A):

$$G(x, y, z) = \frac{1}{2id_x d_y} \sum_{n=-\infty}^{+\infty} \sum_{m=-\infty}^{+\infty} \frac{\exp(i\gamma_{nm}|z|)}{\gamma_{nm}} \exp(i\alpha_n x + i\beta_m y) \quad (4)$$

where

$$\alpha_n = \alpha_0 + n \frac{2\pi}{d_x} \quad (5)$$

$$\beta_m = \beta_0 + m \frac{2\pi}{d_y} \quad (6)$$

$$\gamma_{nm}^2 = k^2 - \alpha_n^2 - \beta_m^2 \quad (7)$$

and choosing  $\gamma_{nm}$  or  $\gamma_{nm}/i$  as a positive number.

It is worth noticing that when  $|z|$  is large enough, the series (4) is rapidly convergent, since the terms of the series decrease exponentially due to the  $\exp(i\gamma_{nm}|z|)$  factor. As a consequence, we can predict that (4) will be numerically efficient as soon as  $|z|$  exceeds a threshold value to be determined in Section 3.3.

### 2.3. First Mixed Form Starting from Spatial Form

In this section, we recall a mixed form series already used in [4]. Starting from (2), we get:

$$G(x, y, z) = G_1(x, y, z) + G_2(x, y, z) \quad (8)$$

with

$$G_1(x, y, z) = -\frac{1}{4\pi} \sum_{n=-\infty}^{+\infty} \sum_{m=-\infty}^{+\infty} \left( \frac{\exp(ikr_{nm})}{r_{nm}} - \frac{\exp(ik\tilde{r}_{nm})}{\tilde{r}_{nm}} \right) \exp(i\alpha_0 nd_x + i\beta_0 md_y) \quad (9)$$

and

$$G_2(x, y, z) = -\frac{1}{4\pi} \sum_{n=-\infty}^{+\infty} \sum_{m=-\infty}^{+\infty} \frac{\exp(ik\tilde{r}_{nm})}{\tilde{r}_{nm}} \exp(i\alpha_0 nd_x + i\beta_0 md_y) \quad (10)$$

where

$$\tilde{r}_{nm} = \sqrt{(x - nd_x)^2 + (y - md_y)^2 + (|z| + u\sqrt{d_x d_y})^2} \quad (11)$$

For small values of the arbitrary positive parameter  $u$ ,  $G_1(x, y, z)$  converges quickly, due to the fact that  $r_{nm}$  and  $\tilde{r}_{nm}$  have the same asymptotic behavior. Moreover, the equality between identities (2) and (4) enables us to transform the second summation in the spectral domain:

$$G_2(x, y, z) = \frac{1}{2id_x d_y} \sum_{n=-\infty}^{+\infty} \sum_{m=-\infty}^{+\infty} \frac{\exp(i\gamma_{nm} (|z| + u\sqrt{d_x d_y}))}{\gamma_{nm}} \exp(i\alpha_n x + i\beta_m y) \quad (12)$$

Note that the parameter  $u$  gives a  $z$ -translation which, following the remark of Section 2.2, enables us to get a fast convergence of  $G_2$  if  $u$  is large enough. Of course, in this case, the convergence of  $G_1$  will be slow. The optimization of this parameter will be discussed in Section 3.2.

### 2.4. Second Mixed Form Starting from Spectral Form

Here again, we recall one mixed form series already used in [9]. The Kummer's transform used in the previous section can be applied to the

spectral form (4), giving:

$$G(x, y, z) = G_3(x, y, z) + G_4(x, y, z) \tag{13}$$

with

$$G_3(x, y, z) = \frac{1}{2id_x d_y} \sum_{n=-\infty}^{+\infty} \sum_{m=-\infty}^{+\infty} \left( \frac{\exp(i\gamma_{nm}|z|)}{\gamma_{nm}} - \frac{\exp(i\tilde{\gamma}_{nm}|z|)}{\tilde{\gamma}_{nm}} \right) \exp(i\alpha_n x + i\beta_m y) \tag{14}$$

and

$$G_4(x, y, z) = \frac{1}{2id_x d_y} \sum_{n=-\infty}^{+\infty} \sum_{m=-\infty}^{+\infty} \frac{\exp(i\tilde{\gamma}_{nm}|z|)}{\tilde{\gamma}_{nm}} \exp(i\alpha_n x + i\beta_m y) \tag{15}$$

putting

$$\tilde{\gamma}_{nm}^2 = -v^2 - \alpha_n^2 - \beta_m^2 \tag{16}$$

where  $v$  is a positive parameter and  $\tilde{\gamma}_{nm}/i$  is a positive number.

Again, the equality between the spatial and the spectral forms (2) and (4), combined with the similarity between (7) and (16) allows us to transform (15) in the spatial domain:

$$G_4(x, y, z) = -\frac{1}{4\pi} \sum_{n=-\infty}^{+\infty} \sum_{m=-\infty}^{+\infty} \frac{\exp(-vr_{nm})}{r_{nm}} \exp(i\alpha_0 n d_x + i\beta_0 m d_y) \tag{17}$$

The convergence of  $G_4$  is due to  $\exp(-vr_{nm})/r_{nm}$  and is faster as  $v$  is larger, but  $G_3$  converges more rapidly as  $v$  is smaller. As a consequence,  $v$  should be numerically optimized (see Section 3.2).

### 3. NUMERICAL STUDY

We have performed numerous tests with various expressions of the Green's functions. It emerges that our goal can be achieved by mean of the three series given by

- Eq. (4),
- Eq. (8), using Eq. (9) and Eq. (12),
- Eq. (13), using Eq. (14) and Eq. (17).

### 3.1. Shanks' Transform

Moreover, on each of the series (9), (12), (14) and (17), we use the Shanks' transform [11, 12] in order to accelerate numerically the convergence. Note that series (4) does not take advantage of Shanks' transform in the range of parameters where this series will be used. In comparison with the method proposed by Jorgenson et al [4] (which is similar to the use of (9) and (12)), we have added the application of Shanks' transform, and we have checked that significant improvements are obtained in all circumstances. Because of the double summation of the series which writes under the general form:

$$S = \sum_{n=-\infty}^{+\infty} \sum_{m=-\infty}^{+\infty} S_{nm}, \quad (18)$$

we must define the way we use for the truncation. Let us call:

$$S_N = \sum_{n=-N}^{+N} \sum_{m=-N}^{+N} S_{nm}. \quad (19)$$

This simple process is interesting since the computation of  $S_{N+1}$  from  $S_N$  takes advantage of all the previous computations. Of course, it could be questionable in the case where  $d_x$  and  $d_y$  are very different. Let us recall the principle of the Shanks' transform. Assuming that  $S_0, S_1 \dots S_{N+1}$  are known, we can compute the  $p$ -order Shanks' transform by:

$$e_p(S_N) = e_{p-2}(S_{N+1}) + \frac{1}{e_{p-1}(S_{N+1}) - e_{p-1}(S_N)}, \quad p = 2 \dots N \quad (20)$$

with initial conditions

$$e_0(S_N) = S_N, \quad e_1(S_N) = \frac{1}{e_0(S_{N+1}) - e_0(S_N)} \quad (21)$$

The successive values of  $e_p(S_N)$ , when  $p$  is an even number, are estimations of  $S$ , and, in our case, converge faster than the initial partial sums  $S_N$ . In order to stop the numerical summations when a given relative error  $\varepsilon$  is reached, we use the following criterion:

$$\left| \frac{e_p(S_0) - e_{p-2}(S_0)}{e_p(S_0)} \right| \leq \varepsilon \quad (22)$$

Note that this convergence test differs from the one used by Singh et al. [9], and is more restrictive. The objective is to avoid that the

procedure stops before the required error is obtained, due to a slow convergence. Moreover, we enforce condition (22) to be verified for at least four consecutive values of  $p$ . For clarity, we will distinguish the error  $\varepsilon$  we wish for, and the obtained error  $\tilde{\varepsilon}$ .

### 3.2. Optimization of the Parameters $u$ and $v$

As mentioned in Sections 2.3 and 2.4, the parameters  $u$  and  $v$  must be optimized. From our numerical studies, it emerges that quite good performances are obtained when  $u$  depends on the parameters  $\lambda = 2\pi/k$ ,  $d_x$ ,  $d_y$  and the error  $\varepsilon$  following the empirical rule:

$$u = (0.005 \log \varepsilon + 0.065) \left( \frac{\lambda}{\sqrt{d_x d_y}} \exp \left( -0.135 \frac{\lambda}{\sqrt{d_x d_y}} \right) \right) + 0.04 \quad (23)$$

In the same way, we found an empirical rule for the determination of  $v$ :

$$v = \frac{0.3 \log \varepsilon + 3.2}{\min(d_x, d_y)} \quad (24)$$

These rules are systematically used in all the following.

### 3.3. Numerical Comparison of the Methods

The goal is to compute the Green's function within the required error  $\varepsilon$ . Among the methods fulfilling this criterion, we select the faster one. Moreover, in order to give to the final routine the largest range of validity, we combine the different methods to cover all the values of  $x$ ,  $y$ ,  $z$  and a wide range of values for  $\lambda$ ,  $\alpha_0$ ,  $\beta_0$ ,  $d_x$ ,  $d_y$  and  $\varepsilon$ . Of course, we cannot illustrate all the different situations. For clarity, we have used a graphic representation that gives a synthetic information.

Figure 1 shows maps of the error  $\tilde{\varepsilon}$  obtained for  $|z|$  varying from  $10^{-6}$  to 1. Due to the pseudo-periodicity of the Green's function, it is sufficient to compute  $G$  in the first cell, i.e.,  $x \in [-d_x/2, d_x/2]$  and  $y \in [-d_y/2, d_y/2]$ . In the left-hand side of the map, we fix  $y = 0$  and vary  $x$  between  $-d_x/2$  and 0, whereas in the right-hand side, we take  $y = x$ , and vary  $x$  between 0 and  $d_x/2$ . The other useful parameters are  $\lambda = d_x = d_y = 1$ ,  $\alpha_0 = k \sin(\pi/4)$ ,  $\beta_0 = 0$  and  $\varepsilon = 10^{-6}$ . Figure 1a is computed using Eq. (8), Figure 1b is computed using Eq. (13) and Figure 1c is computed using our numerical code, which automatically chooses the proper method. In the upper band on Fig. 1c (i.e.,  $\log |z| > -1.15$  above the white line), the spectral form (Eq. (4)) is used. We have not shown the entire map obtained with this method. From the remark in Section 2.2, it is clear that the

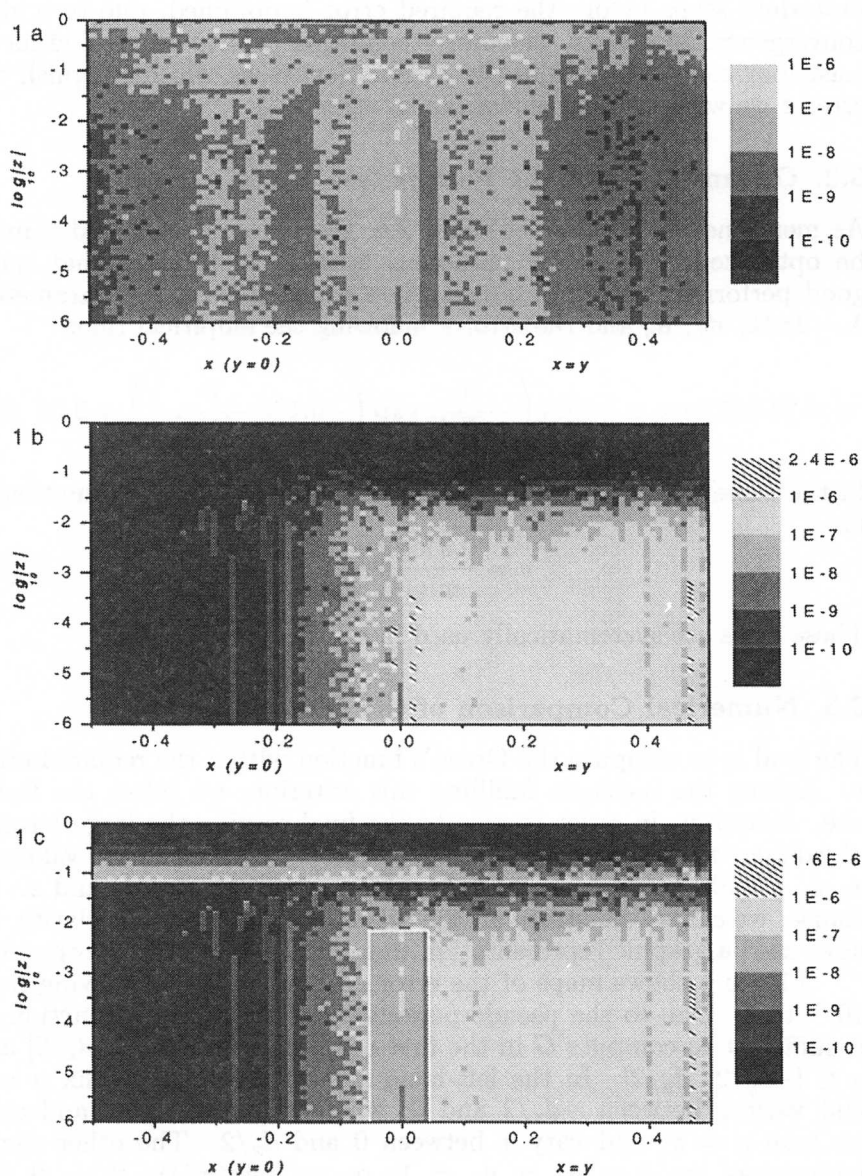


**Figure 1.** Error maps. 1a: from Eq. (8). 1b: from Eq. (13). 1c: from our code. Shanks' transformation is applied on series (8) and (13). If  $\tilde{\varepsilon} > \varepsilon$ , the legends show a hatched region whose lower limit is equal to  $\varepsilon$ , and whose upper limit is the maximum error  $\tilde{\varepsilon}$  among all the calculations of the map.



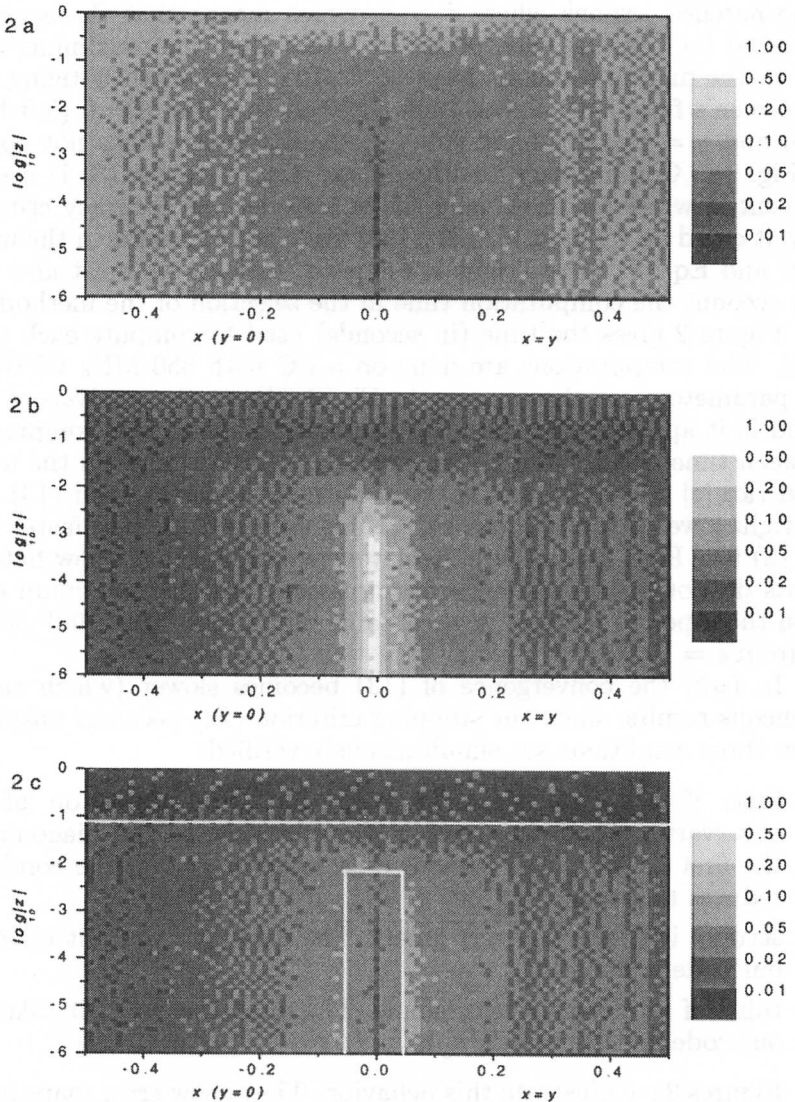
method is efficient for large values of  $|z|$  only. In Figure 1b, we notice some hatched regions where  $\tilde{\varepsilon} > \varepsilon$ , which means that the accuracy we asked for has not been obtained. Note that the maximum value of  $\tilde{\varepsilon}$  in the map is equal to  $2.4 \times 10^{-6}$ . It is also worth noticing that the Green's function behaves differently on the lines  $y = 0$  (left-hand side) and  $y = x$  (right-hand side). This asymmetry does not appear on Fig. 1a. Coming back to Fig. 1c, we note that Eq. (8) is used in the central white rectangle only. If we consider the accuracy criterion only, it could be thought that Eq. (13) gives better results in the upper part, and Eq. (8) in the right lower part. In fact, we must also take into account the computation time in the selection of the method.

Figure 2 gives the time (in seconds) used to compute each value of  $G$ . The computations are done on a PC with 350 MHz CPU and the parameters are the same as in Fig. 1. From the analysis of Fig. 1 and 2, it appears that the numerical code gives a good compromise between time and accuracy. For instance, it is clear that in the upper band ( $\log |z| > -1.15$ ), the spectral form (4) is faster than (13). On the right lower side of Fig. 1c, Eq. (13) is used because it is faster than Eq. (8) (see Figs. 2a and 2b). However, we can see that a few hatched points do not satisfy the accuracy criterion, but the maximum error upon these points remains in acceptable limits ( $\tilde{\varepsilon} = 1.6 \times 10^{-6}$ , not so far from  $\varepsilon = 10^{-6}$ ).

In fact, the convergence of (13) becomes slower (which causes erroneous results, since our stopping criterion (22) becomes unsuited) when three conditions are simultaneously verified:

- first, if  $x/d_x$  get close to  $y/d_y$  (i.e., the projection of the observation point on the  $x, y$  plane is close to the diagonals of the first cell). In the present case where  $d_x = d_y$ , the condition reduces to  $x \approx y$ ,
- second, if  $\varepsilon$  becomes very small. The quantitative limit taken by our code is  $5 \times 10^{-7}$ ,
- third, if  $|z|$  becomes very small. The quantitative limit taken by our code is  $0.07 \max(d_x, d_y)$ ,

Figures 3a–c illustrate this behavior. They show error maps in the plane  $z = 0$ , for the same parameters as previously, except  $\varepsilon = 10^{-8}$ . From Figure 3b, we see that the slow convergence of (13) induces erroneous results that are due to the fact that the criterion used to stop the numerical summations fails. In this case, Fig. 3c shows that our numerical code uses Eq. (8), thus giving more importance to accuracy than to quickness. Note that in the case of Figures 1 and 2 ( $\varepsilon = 10^{-6}$ ) the problem is not so critical, and Eq. (13) can be used for  $x = y$ .



**Figure 2.** Computation time. 1a: from Eq. (8). 1b: from Eq. (13). 1c: from our code. Shanks' transformation is applied on series (8) and (13). Note that some small differences in the computation time for the same point appear (for instance in the central region between maps 2a and 2c) due to uncertainty on the time measurement.

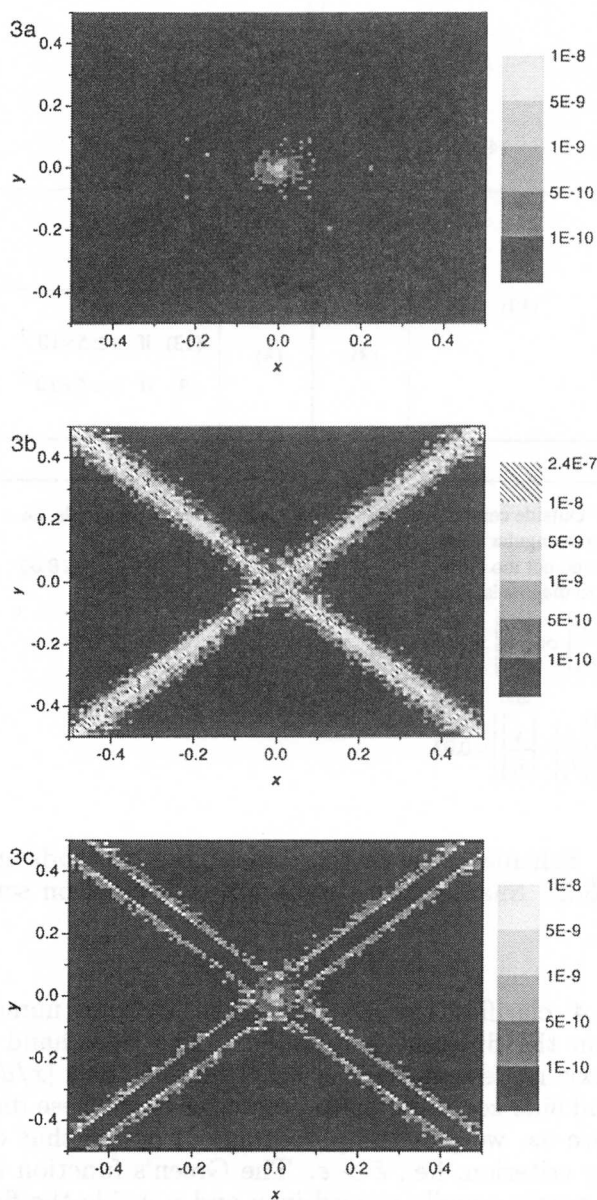


**Figure 3.** Error maps versus  $x$  and  $y$ , for  $z = 0$ . 3a: from Eq. (8). 3b: from Eq. (13). 3c: from our code. Shanks' transformation is applied on series (8) and (13). If  $\tilde{\varepsilon} > \varepsilon$ , the legends show a hatched region whose lower limit is equal to  $\varepsilon$ , and whose upper limit is the maximum error  $\tilde{\varepsilon}$  among all the calculations of the map.

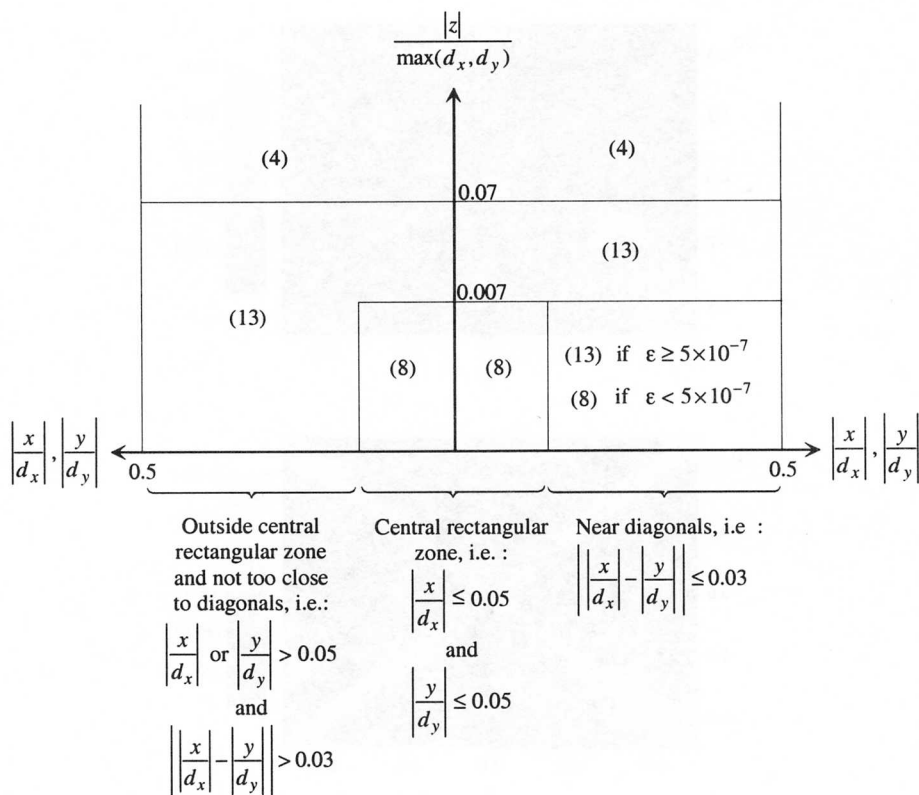


**Figure 4.** Schematic representation of the methods used by our numerical code. Shanks' transformation is applied on series (8) and (13).

Figure 4 clarifies the choices taken by our numerical code, depending on the different parameters. The right-hand side of the horizontal axis represents regions near the diagonals  $|x/d_x| = |y/d_y|$ . The left-hand side corresponds to points far from these diagonals.

In Figure 5a, we plot the percentage of points that do not meet the accuracy criterion, i.e.,  $\tilde{\varepsilon} > \varepsilon$ . The Green's function is computed over 10,000 points equally spaced in  $x$  and  $y$  inside the first cell, and logarithmically spaced from  $z = 10^{-6}$  to  $z = 1$ . The parameters remain the same as previously. The worse results are obtained when using Eq. (8) without Shanks' transform. This method is very close to the one proposed in [4]. Using (13), Shanks' transform gives good results as long as  $\varepsilon > 10^{-6}$ , but the number of false results increases as  $\varepsilon$

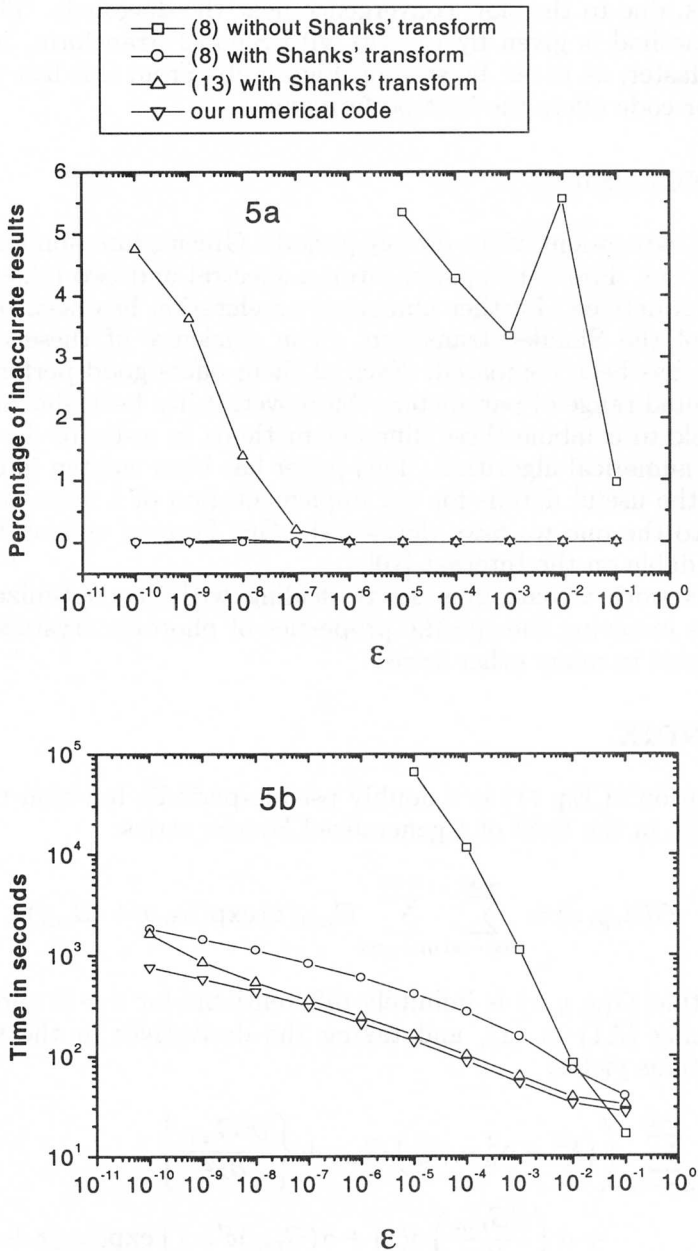


**Figure 5.** Comparison between the different methods over 10,000 points. 5a: percentage of inaccurate results versus  $\epsilon$ . 5b: computation time.

decreases, due to the slow convergence near the diagonals. The more robust method is given by Eq. (8) with Shanks' transform, but it is not the faster, as it can be seen on Figure 5b. From this last point of view, our code offers the best performances.

#### 4. CONCLUSION

Different expressions of the doubly periodic Green's function have been sketched out. From the spatial form, a spectral and two mixed forms have been derived. Further numerical acceleration has been obtained by use of the Shanks' transform. The efficiency of these different methods has been compared. Each of them offers good performances for a limited range of parameters. Moreover, it has been shown that it is possible to combine these different methods in order to develop an efficient numerical algorithm. This paper has been written in order to give all the useful details for the implementation of a numerical code similar to the one we have developed. Our Fortran version is freely downloadable on the Internet [10].

This work is part of a study dealing with the optimization of antennas involving the specific properties of photonic crystals, but it can be used in many other areas.

#### APPENDIX

The solution of Eq. (1) is a doubly pseudo-periodic function that can be written in the form of a generalized Fourier series:

$$G(x, y, z) = \sum_{n=-\infty}^{+\infty} \sum_{m=-\infty}^{+\infty} G_{nm}(z) \exp(i\alpha_n x + i\beta_m y) \quad (\text{A1})$$

Noting that  $G(x, y, z)$  is infinitely differentiable for  $z > 0$  and  $z < 0$ , introducing (A1) in (1), and taking the derivatives in the sense of distributions yields:

$$\begin{aligned} & \sum_{n=-\infty}^{+\infty} \sum_{m=-\infty}^{+\infty} \left( (k^2 - \alpha_n^2 - \beta_m^2) G_{nm} + \left\{ \frac{\partial^2 G_{nm}}{\partial z^2} \right\} \right. \\ & \quad \left. + \sigma \left( \frac{\partial G_{nm}}{\partial z} \right) \delta(z) + \sigma(G_{nm}) \delta'(z) \right) \exp(i\alpha_n x + i\beta_m y) \\ & = \delta(z) \sum_{n=-\infty}^{+\infty} \sum_{m=-\infty}^{+\infty} \delta(x - nd_x) \delta(y - md_y) \exp(i\alpha_0 x + i\beta_0 y) \quad (\text{A2}) \end{aligned}$$

where  $\left\{\frac{\partial^2 f}{\partial z^2}\right\}$  denotes the second derivative of  $f$  without precaution,  $\sigma(f)$  the jump of  $f$  for  $z = 0$ , and  $\delta'$  the derivative of the Dirac's distribution. Note that in the right-hand member of (A2) we have replaced  $nd_x$  by  $x$  and  $md_y$  by  $y$ . This is allowed by the presence of the factors  $\delta(x - nd_x)$  and  $\delta(y - md_y)$ . Using the well known identity:

$$\sum_{n=-\infty}^{+\infty} \delta(x - nd_x) = \frac{1}{d_x} \sum_{n=-\infty}^{+\infty} \exp\left(2i\pi n \frac{x}{d_x}\right) \quad (\text{A3})$$

Eq. (A2) writes:

$$\begin{aligned} & \sum_{n=-\infty}^{+\infty} \sum_{m=-\infty}^{+\infty} \left( (k^2 - \alpha_n^2 - \beta_m^2) G_{nm} + \left\{ \frac{\partial^2 G_{nm}}{\partial z^2} \right\} \right. \\ & \quad \left. + \sigma\left(\frac{\partial G_{nm}}{\partial z}\right) \delta(z) + \sigma(G_{nm}) \delta'(z) \right) \exp(i\alpha_n x + i\beta_m y) \\ & = \sum_{n=-\infty}^{+\infty} \sum_{m=-\infty}^{+\infty} \frac{\delta(z)}{d_x d_y} \exp(i\alpha_n x + i\beta_m y) \end{aligned} \quad (\text{A4})$$

which means that for each  $(n, m)$ :

$$\gamma_{nm}^2 G_{nm} + \left\{ \frac{\partial^2 G_{nm}}{\partial z^2} \right\} + \sigma\left(\frac{\partial G_{nm}}{\partial z}\right) \delta(z) + \sigma(G_{nm}) \delta'(z) = \frac{1}{d_x d_y} \delta(z) \quad (\text{A5})$$

giving us the three following relations:

$$\sigma(G_{nm}) = 0 \quad (\text{A6})$$

$$\sigma\left(\frac{\partial G_{nm}}{\partial z}\right) = \frac{1}{d_x d_y} \quad (\text{A7})$$

$$\gamma_{nm}^2 G_{nm} + \left\{ \frac{\partial^2 G_{nm}}{\partial z^2} \right\} = 0 \quad (\text{A8})$$

Equation (A6) means that  $G_{nm}(z)$  is continuous in  $z = 0$ , whereas from (A8) we can write:

$$\text{for } z > 0, \quad G_{nm} = A_{nm} \exp(i\gamma_{nm} z) + B_{nm} \exp(-i\gamma_{nm} z) \quad (\text{A9})$$

$$\text{for } z < 0, \quad G_{nm} = C_{nm} \exp(i\gamma_{nm} z) + D_{nm} \exp(-i\gamma_{nm} z) \quad (\text{A10})$$

The outgoing wave condition imposes that  $B_{nm} = C_{nm} = 0$ , and the continuity of  $G_{nm}$  gives  $A_{nm} = D_{nm}$ . Finally, (A7) fixes the value:

$$A_{nm} = D_{nm} = \frac{1}{2id_x d_y \gamma_{nm}} \quad (\text{A11})$$

Thus the expression of the Green's function is:

$$G(x, y, z) = \frac{1}{2id_x d_y} \sum_{n=-\infty}^{+\infty} \sum_{m=-\infty}^{+\infty} \frac{\exp(i\gamma_{nm}|z|)}{\gamma_{nm}} \exp(i\alpha_n x + i\beta_m y) \quad (\text{A12})$$

## REFERENCES

1. Nicorivici, N. A., R. C. Mc Phedran, and R. Petit, "Efficient calculation of the Green's function for electromagnetic scattering by gratings," *Phys. Rev. E*, Vol. 49, 4563–4577, 1994.
2. Tayeb, G., "The method of fictitious sources applied to diffraction gratings," *Applied Computational Electromagnetic Society (ACES) Journal*, Vol. 9, 90–100, 1994.
3. Wallinga, G. S., E. J. Rothwell, K. M. Chen, and D. P. Nyquist, "Efficient computation of the two-dimensional periodic Green's function," *IEEE Trans. Antennas Propagat.*, Vol. 47, 895–897, 1999.
4. Jorgenson, R. E. and R. Mittra, "Efficient calculation of the free-space periodic Green's function," *IEEE Trans. Antennas Propagat.*, Vol. 38, 633–642, 1990.
5. Singh, S. and R. Singh, "On the use of Shanks' transform to accelerate the summation of slowly convergent series," *IEEE Trans. Microwaves Theory Tech.*, Vol. 39, 608–610, 1991.
6. Singh, S. and R. Singh, "On improving the computational efficiency in problems involving one- and two-dimensional periodicity," *J. Electromagn. Waves Applicat.*, Vol. 6, 911–919, 1992.
7. Singh, S. and R. Singh, "On the use of  $\rho$ -algorithm in series acceleration," *IEEE Trans. Antennas Propagat.*, Vol. 39, 1514–1517, 1991.
8. Yasumoto, K. and K. Yoshitomi, "Efficient calculation of lattice sums for free-space periodic Green's function," *IEEE Trans. Antennas Propagat.*, Vol. 47, 1050–1055, 1999.
9. Singh, S., W. F. Richards, J. R. Zinecker, and D. R. Wilton, "Accelerating the convergence of series representing the free space periodic Green's function," *IEEE Trans. Antennas Propagat.*, Vol. 38, 1958–1962, 1990.
10. <http://www.infrance.net/fresnel/>
11. Shanks, D., "Non-linear transformations of divergent and slowly convergent sequences," *J. Math. Phys.*, Vol. 34, 1–42, 1955.



12. Wytt, F., "On a device for computing the  $e_m(S_n)$  transformation," *Math. Tables and Aids to Comp.*, Vol. 10, 91–96, 1956.

**Nicolas Guérin** was born in Tarbes, France, on April 24, 1977. He received the M.S. degree in physics in 1998 from the University of Paul Sabatier, Toulouse, France. He is currently working toward the Ph.D. degree in the Institut Fresnel, Marseille. He is engaged in research on numerical methods applied to antennas and scattering problems.

**Stefan Enoch** was born in Aix en Provence, France, on May 18, 1970. He is qualified from the École Nationale Supérieure de Physique de Marseille (1994). His thesis (1997) was on second-harmonic generation by gratings and rough surfaces. He is currently Maître de Conférences (Assistant Professor) in the University of Aix-Marseille. He is mainly involved in the theoretical and numerical study of photonic crystals.

**Gérard Tayeb** was born in Marseille, France, on November 11, 1959. He graduated from the Ecole Normale Supérieure de l'Enseignement Technique and received the Agrégation of Physics in 1981. He joined the Laboratoire d'Optique Électromagnétique in 1985, and he is currently Professor in the University of Aix-Marseille. His doctoral thesis (1990) dealt with diffraction by gratings, development of new methods, and application to anisotropic structures. He is now mainly interested in the investigation of photonic crystals properties. He is author or co-author of 18 refereed journal articles, 20 conference papers, and 2 book chapters.